

Effect of wind stress forcing on ocean dynamics at air-sea interface

Hussein YAHIA^{†1}, Veronique GARÇON², Joel SUDRE², Christophe MAES³

¹Research Center INRIA Bordeaux - South West, Talence 33405, France

²CNRS, LEGOS Laboratory, Toulouse 31400, France

³Brest University, CNRS, IRD, IFREMER, LOPS, IUEM, Brest 29238, France

E-mail: hussein.yahia@inria.fr; veronique.garcon@legos.obs-mip.fr; joel.sudre@legos.obs-mip.fr; christophe.maes@ird.fr

Received Nov. 29, 2017; Revision accepted Mar. 16, 2018; Crosschecked Aug. 9, 2018

Abstract: We evidence and study the differences in turbulence statistics in ocean dynamics carried by wind forcing at the air-sea interface. Surface currents at the air-sea interaction are of crucial importance because they transport heat from low to high latitudes. At first order, oceanic currents are generated by the balance of the Coriolis and pressure gradient forces (geostrophic current) and the balance of the Coriolis and the frictional forces dominated by wind stress (Ekman current) in the surface ocean layers. The study was conducted by computing statistical moments on the shapes of spectra computed within the framework of microcanonical multi-fractal formalism. Remotely sensed daily datasets derived from one year of altimetry and wind data were used in this study, allowing for the computation of two kinds of vector fields: geostrophy with and geostrophy without wind stress forcing. We explore the statistical properties of singularity spectra computed from velocity norms and vorticity data, notably in relation with kurtosis information to underline the differences in the turbulent regimes associated with both kinds of velocity fields.

Key words: Ocean dynamics; Remote sensing; Turbulence; Signal processing; Multi-fractal formalism

<https://doi.org/10.1631/FITEE.1700797>


CLC number: TP391

1 Introduction and motivation

Due to the adequate synoptic picture of ocean circulation provided by altimetry techniques (Chelton et al., 2001), refined analysis of turbulent surface ocean dynamics has become a tractable field of research. However, existing ocean circulation models which are used to compute ocean dynamics operate at spatial scales far superior to the lower limit of the ocean's inertial range. Consequently, they cannot be used presently to provide a precise quantitative analysis of the differences in turbulence statistics in space, time (seasonal time scales), and observation scales (Lee et al., 2010). A quantitative

description of ocean surface turbulence statistics at different spatial and time scales finds interesting applications in oceanography. At mesoscale, geostrophic eddies dominate the turbulent motion, with radii between 10 and 100 km, with notable effects on mixing, heat, and climatically active tracers (Mashayek et al., 2017). Submesoscale turbulence is a very active field of research, with coherent structures less than one kilometer in size down to a few meters, and a likely role in vertical mixing. Below this, the turbulent properties and characteristics of ocean dynamics close to the lower limit of the inertial range are unknown. A quantitative evaluation of the spatial and seasonal variability in the turbulent properties of ocean dynamics is a promising field of research, notably in relation with upwelling and air/sea exchanges at the interface (Hernández-Carrasco et al., 2015).

[†] Corresponding author

 ORCID: Hussein YAHIA, <http://orcid.org/0000-0002-4284-096X>

© Zhejiang University and Springer-Verlag GmbH Germany, part of Springer Nature 2018

In this paper, we study the variations in the statistics of ocean dynamics turbulence directly from the acquired data, with a focus on mesoscale oceanic data. Our goal is to provide quantitative evaluation of wind stress forcing effects on mesoscale ocean dynamics.

2 Surface ocean dynamics

We use the surface ocean dynamics product at the $1/4^\circ$ as described in Sudre et al. (2013). Our data covers one year of daily acquisitions from 2010. Using these datasets, the central hypothesis is to estimate the first-order current as the sum of geostrophic and wind driven components:

1. Geostrophic current is determined from the absolute dynamic topography.
2. Equator singularity is solved with semi-geostrophy approximation.
3. Ekman current is estimated by fitting a simple Ekman model based on the residual $\mathbf{v}_{\text{drifter}} - \mathbf{v}_{\text{geos}}$.
4. Validation is performed with the shipboard acoustic Doppler current profiler (ADCP), equatorial moorings, surface velocity program (SVP) drifters, and surface displacement Argo floats.

Using these data, we calculate the norm of geostrophic current with and without Ekman currents and the associated vorticity for the following four areas of study: (1) Agulhas retroflection; (2) Gulf-Stream area; (3) Peru-Chile area; (4) Brazil-Malvinas area.

In Fig. 1, we display the norm of the geostrophic surface current for the 1st January 2010. For each daily acquisition from 2010, we obtain the norm of the oceanic velocity field with and without the Ekman currents. From these data we obtain the vorticity of the geostrophic velocity field, again with and without Ekman currents: $\omega = \nabla \wedge \mathbf{v}$, where ' \wedge ' denotes the vector product.

3 Method

In the phenomenological description of turbulence, a fundamental problem is the study of the intermittency of the energy transfer (Benzi et al., 1984; Parisi and Frisch, 1985; She and Leveque, 1994; Frisch, 1995). This leads to the definition of the multi-fractal formalism for a quantitative and descriptive account of the breaking of self-similarity of

the velocity random field $\mathbf{v}(\mathbf{x})$ at inertial range. In this formalism, intermittency is a direct consequence of the irregular geometrical structure of the repartition of energy transfer, which takes places over a spatial set of multi-fractal nature.

In the K41 theory, at each point \mathbf{x} , the difference is $\|\mathbf{v}(\mathbf{x} + \mathbf{r}) - \mathbf{v}(\mathbf{x})\| \sim r^h$ ($r \rightarrow 0$) with a same value for every \mathbf{x} : $h = 1/3$, which implies that the energy dissipation scalar field $\varepsilon(\mathbf{x})$ is smooth and the scaling law for the velocity random field $\Delta \mathbf{v}(\mathbf{x}, l) \doteq l^{1/3} \Delta \mathbf{v}(\mathbf{x}, r)$ with $\Delta \mathbf{v}(\mathbf{x}, r) = \mathbf{v}(\mathbf{x} + \mathbf{r}) - \mathbf{v}(\mathbf{x})$ and \doteq means equality in law. Yet, the energy dissipation field is intermittent and, in fact, the scaling law occurs over a hierarchy of dense sets of multi-fractal nature. Moreover, the notion of a unique singularity exponent h must be extended and replaced by singularity exponents varying from point to point (Turiel et al., 2008).

In the canonical description of multi-fractality (Arneodo et al., 1995), one considers the expectation (moment) $\mathbb{E}[\|\mathbf{v}(\mathbf{x} + \mathbf{r}) - \mathbf{v}(\mathbf{x})\|^q] = \mathbb{E}[\|\Delta \mathbf{v}(\mathbf{x}, r)\|^q] \sim r^{\zeta(q)}$ with $\zeta(q)$ being a nonlinear function of the order moment q (anomalous scaling). If \mathcal{F}_h denotes the set of points \mathbf{x} such that $\|\mathbf{v}(\mathbf{x} + \mathbf{r}) - \mathbf{v}(\mathbf{x})\| \sim r^h$, then the mapping $h \mapsto D(\mathcal{F}_h)$ is called the singularity spectrum, with $D(\mathcal{F}_h)$ being the Hausdorff dimension of the set \mathcal{F}_h . The multi-fractal formalism can be extended outside the domain of fluid turbulence to any function or measure, or to any complex signal (Boffetta et al., 2002; Turiel et al., 2014). From that viewpoint, the singularity spectrum previously defined appears as a particular case (the case where the signal under study is the mapping $\mathbf{x} \mapsto \|\mathbf{v}(\mathbf{x})\|$) of a more general setting available for general functions or measures, and the effective computation of singularities is achieved with wavelets.

Let $\psi : \mathbb{R} \rightarrow \mathbb{R}$ be a specific function called 'analyzing wavelet', $s > 0$ a strictly positive real number (the 'scale'), and ψ_s the 'symmetrized scaled version' of ψ :

$$\psi_s(\mathbf{x}) = \frac{1}{\sqrt{s}} \psi\left(-\frac{\mathbf{x}}{s}\right). \quad (1)$$

Let $\phi_{\mathbf{a}}(\mathbf{x}) = \mathbf{x} - \mathbf{a}$ be a translation in the signal domain and $\gamma_s(\mathbf{x}) = s\mathbf{x}$ the scale operator. The continuous wavelet transform (CWT) of a signal $f \in L^2(\mathbb{R})$ is the function of the variables: $\mathbf{a} \in \mathbb{R}$

(position) and $s > 0$ (scale):

$$(\mathcal{W}f)(\mathbf{a}, s) = \frac{1}{\sqrt{s}} \langle f | \psi \circ \gamma_{1/s} \circ \phi_{\mathbf{a}} \rangle = f * \overline{\psi_s}(\mathbf{a}), \quad (2)$$

where f is correlated with the two-indexed family $\frac{1}{\sqrt{s}} \psi \circ \gamma_{1/s} \circ \phi_{\mathbf{a}}$ of ‘atoms’ depending on position and scale. If the analyzing wavelet has n_ψ vanishing moments, then $(\mathcal{W}f)(\mathbf{a}, s) \sim s^{h(\mathbf{a})} s \rightarrow 0$, where $h(\mathbf{a})$ is the singularity of function f at \mathbf{a} , provided $n_\psi > h(\mathbf{a})$. There are many ways of computing a singularity spectrum in the canonical multi-fractal formalism. The most elementary way, although not efficient numerically, consists in evaluating $h \mapsto D(\mathcal{F}_h)$ from the CWT. Without going into details, we mention here the basic ideas in order to get a grasp of the multi-fractal formalism and to introduce more sophisticated methods of computing a singularity spectrum. A ‘partition function’ is defined with the CWT: $\mathcal{Z}(q, s) = \int_{\mathbb{R}} |(\mathcal{W}f)(\mathbf{x}, s)|^q d\mathbf{x}$. It can be shown that, in the case of multi-fractal signals, one has $\mathcal{Z}(q, s) \sim s^{\tau(q)}$, $s \rightarrow 0$, and the singularity spectrum can be derived as a Legendre transform of $q \mapsto \tau(q)$: $D_h = D(\mathcal{F}_h) = \min_q (qh + \tau(q) + D_f)$ with D_f being a constant equal to the dimension of the support of singularities of f . When $\tau(q)$ is smooth, one has $q = \frac{dD_h}{dh}$, $\tau(q) = qh - D_h + D_f$. The general shape of the singularity spectrum D_h is given

in Fig. 2. The left part of the spectrum is particularly interesting, as it is associated with the strongest transitions in signal f .

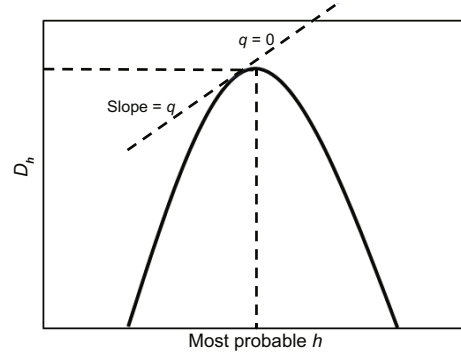


Fig. 2 General shape of the singularity spectrum $h \mapsto D_h$ as the Legendre transform of $q \mapsto \tau(q)$

As we explained earlier, this method of computing a singularity spectrum is not the most accurate and it has been extended and modified in various directions: the wavelet transform modulus maxima (WTMM) and log-cumulant analysis method (Venu-gopal et al. (2006) and the references herein); we will not expand upon the canonical formalism in this work, but rather turn to a micro-canonical formulation, which is able to compute alternate ‘spectra’, based on the log-histogram approach (Turiel et al., 2008), with high numerical precision and an efficient

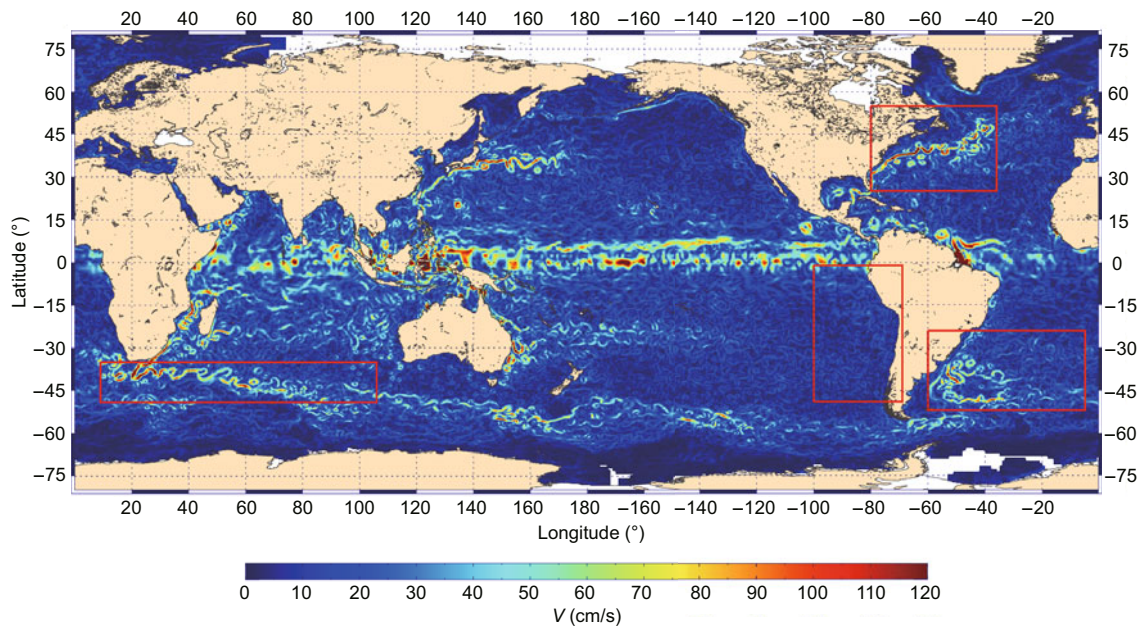


Fig. 1 Norm of the geostrophic surface current for the 1st January 2010. The red rectangles represent the four areas of study. References to color refer to the online version of this figure

algorithm. In this method, we consider the gradient measure associated with signal f , although f is not differentiable. Moreover, in the case of acquired data, which consists of finite signals acquired at fixed spatial resolution, we consider the data provided by ∇f computed either by finite differences or by taking the inverse Fourier transform of $(-i\mathbf{x}\hat{f}, -i\mathbf{y}\hat{f})$ (\hat{f} : Fourier transform of f). The gradient measure μ is the measure on \mathbb{R}^2 whose density is $\nabla f : d\mu = \nabla f d\lambda$ (λ : Lebesgue measure on \mathbb{R}^2). Let $\mathcal{B}_r(\mathbf{x})$ be the ball of radius r centered at point \mathbf{x} . Then one has

$$\mu(\mathcal{B}_r(\mathbf{x})) = \alpha(\mathbf{x})r^{h(\mathbf{x})} + o(r^{h(\mathbf{x})})(r \rightarrow 0), \quad (3)$$

with $h(\mathbf{x})$ being the singularity exponent of measure μ at \mathbf{x} . For most signals, the exponent $h(\mathbf{x})$ is an independent prefactor $\alpha(\mathbf{x})$. For small scales r (such that the $o(r^{h(\mathbf{x})})$ term becomes negligible), the dependence on the scale parameter is concentrated in the factor $r^{h(\mathbf{x})}$, so the knowledge of the exponent $h(\mathbf{x})$ allows interpretation of the type of transition which is taking place at \mathbf{x} . Points are classified accordingly by the ‘transition fronts’ or ‘singularity manifolds’ of the system. We denote by \mathcal{F}_h the singularity manifold associated to the singularity value h , defined as follows (Turiel et al., 2008):

$$\mathcal{F}_h = \{\mathbf{x} : h(\mathbf{x}) = h\}. \quad (4)$$

As in canonical formulation, we denote $D(h)$ the Hausdorff dimension of manifold \mathcal{F}_h . We retrieve in the microcanonical formalism a spectrum in the form of the mapping quantity $h \mapsto D(h)$, and the canonical exponents $\tau(p)$, associated to the structure functions of order p , are related to the spectrum $D(h)$ in the following way:

$$\tau(p) = \inf_h (ph + 2 - D(h)). \quad (5)$$

Conversely, if $D(h)$ is convex, the spectrum can be retrieved from the canonical exponents by applying a Legendre transform:

$$D(h) = \inf_p (ph + 2 - \tau(p)). \quad (6)$$

Suppose that we evaluate the singularity at a resolution scale r_0 which is small enough (typically the scale of the acquisition). The distribution of

singularities at this scale, $\rho_{r_0}(h)$, must verify

$$\rho_{r_0}(h) = A_0 r_0^{2-D(h)} + o(r_0^{2-D(h)}). \quad (7)$$

Consequently, provided that we know the resolution scale r_0 , we can retrieve a spectrum by just evaluating the empirical histogram of singularity exponents. We will further assume, to simplify the analysis, that there exists a singularity manifold \mathcal{F}_{h_1} of maximum dimensionality, $D(h_1) = 2$. Applying such assumption to Eq. (7), we obtain the following estimate of the spectrum:

$$D(h) = 2 - \frac{\log(\rho_{r_0}(h)/\rho_{r_0}^M)}{\log r_0}, \quad (8)$$

where $\rho_{r_0}^M = \max_h(\rho_{r_0}(h))$. Eq. (8) is referred to as the ‘histogram method’ for the evaluation of the singularity spectrum. In the rest of this article, we rely entirely on this method of computing the spectra.

4 Results

Fig. 3 shows the absolute vorticity of geostrophic and Ekman currents for the 1st January 2010 taken out of the experimentation dataset and the corresponding singularity exponents. On the left part, Fig. 4 shows, for the 1st January 2010 in the Agulhas retroflection area, the norm of geostrophic currents (Fig. 4a), the singularity exponents (Fig. 4c), and the associated spectrum (Fig. 4e). On the right part, Figs. 4b, 4d, and 4f show the same data for the norm of the geostrophic part and Ekman currents. Readers will notice the difference in the left part of the spectra, which is the most informative part of the spectra with respect to the strongest transition fronts and coherent structures, and consequently to the statistics of oceanic turbulence, as recorded in the data. This difference is quantitatively expressed by the marked difference in kurtosis between the two spectra.

We now apply the methodology described in the last section on our experimental dataset, made from one year of daily data. The data used is made of altimetry and wind data, both remotely sensed (Arbic et al., 2013; Sudre et al., 2013) for an in-depth description of the datasets and derived products. We compute, for each of the four areas as shown in Fig. 1, the monthly mean kurtosis of the spectra of geostrophic norm and the monthly mean kurtosis

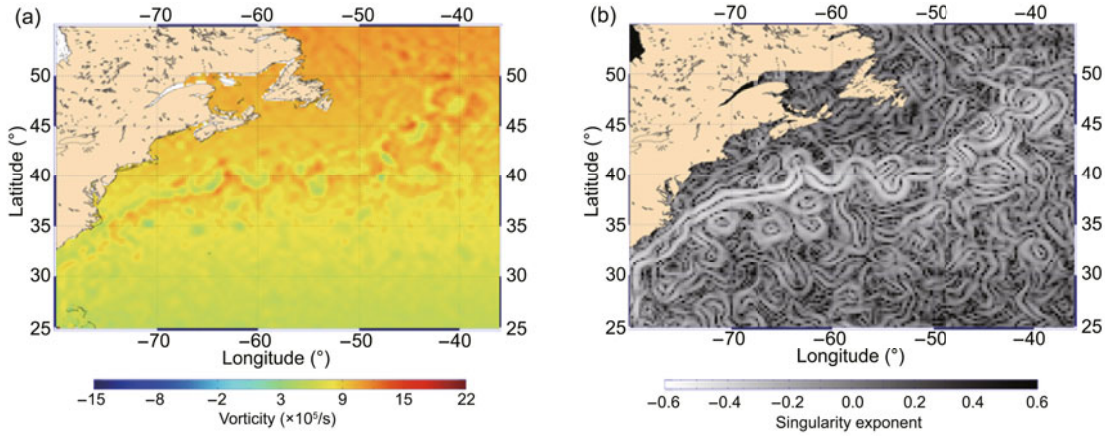


Fig. 3 Absolute vorticity of geostrophic and Ekman currents (a) and corresponding singularity exponents (b) for the 1st January 2010. References to color refer to the online version of this figure

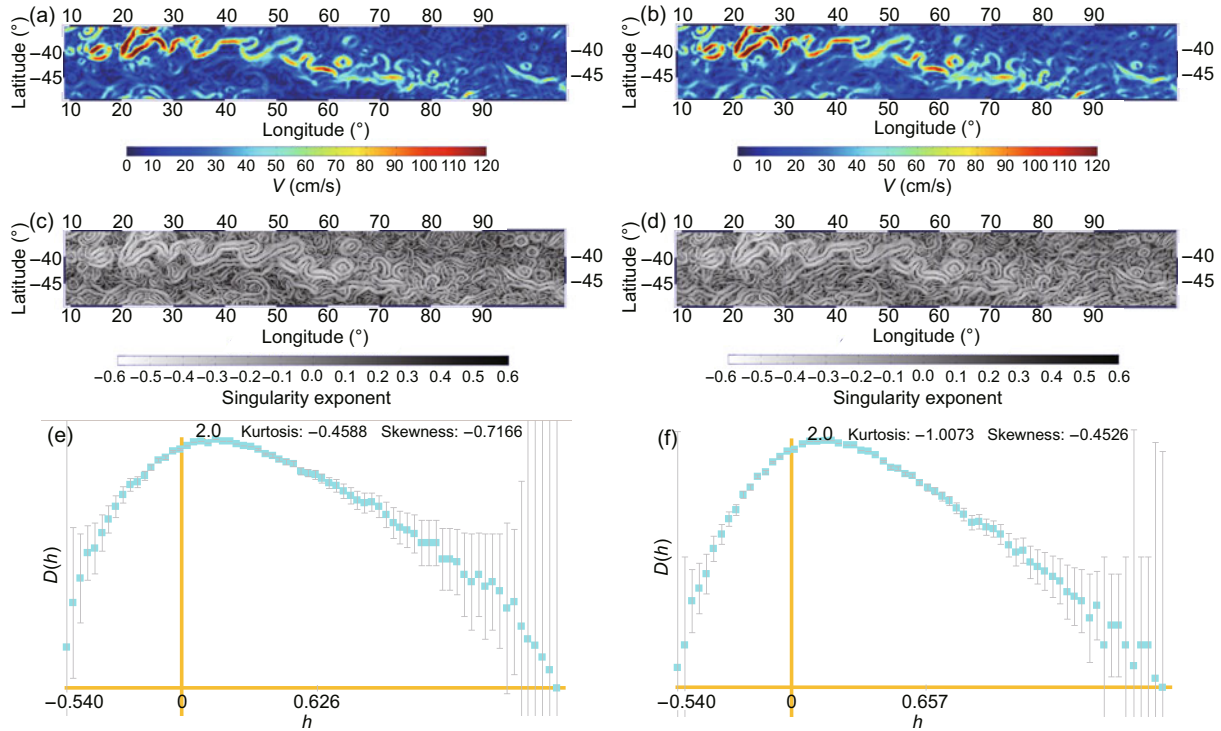


Fig. 4 For the 1st January 2010 in the Agulhas area: norm of geostrophic currents (a), singularity exponents (c), and associated spectrum (e); norm of geostrophic and Ekman currents (b), singularity exponents (d), and associated spectrum (f). Error bars in the spectra are computed using the method described in Turiel et al. (2006). References to color refer to the online version of this figure

of the singularity spectra of geostrophic vorticity. If $\mathbf{a} = [a_1, a_2, \dots, a_n]$ is a discrete signal, we use the ‘excess kurtosis’ defined by

$$\kappa = \frac{1}{\sigma^4} \sum_{i=1}^n \frac{(a_i - \mathbb{E}[\mathbf{a}])^4}{n}, \quad (9)$$

where $\mathbb{E}[\mathbf{a}]$ is the mean value of \mathbf{a} and σ is the stan-

dard deviation. With this definition, a standard normal distribution has a kurtosis of zero. Positive kurtosis means a ‘heavy tailed’ distribution and negative kurtosis a ‘light tailed’ distribution. Neat differences in kurtosis (in particular, positive and negative) mean different organizations of the multi-fractal hierarchy, and statistical differences in the turbulence regime. Figs. 5–8 show the results of the anal-

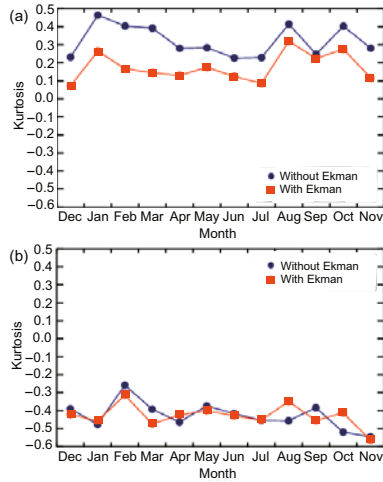


Fig. 5 Results of Gulf Stream area: monthly mean kurtosis of the spectra of geostrophic norm (a) and geostrophic vorticity (b)

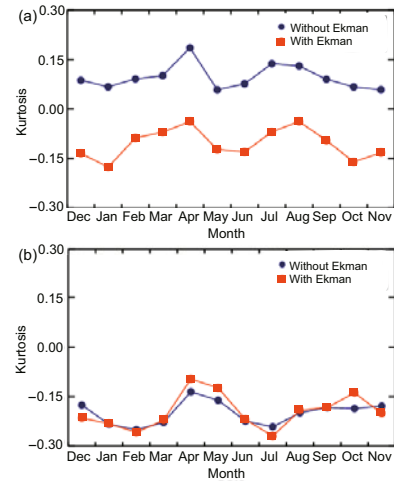


Fig. 7 Results of Agulhas area: monthly mean kurtosis of the spectra of geostrophic norm (a) and geostrophic vorticity (b)

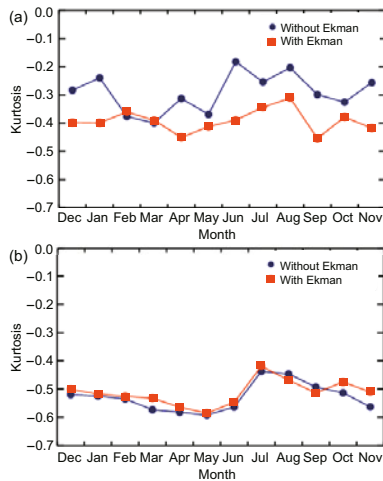


Fig. 6 Results of Brazil-Malvinas area: monthly mean kurtosis of the spectra of geostrophic norm (a) and geostrophic vorticity (b)

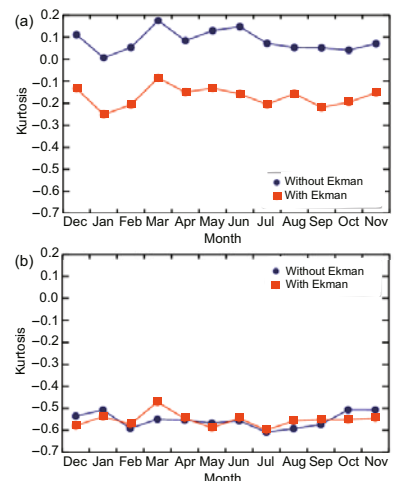


Fig. 8 Results of Peru-Chile area: monthly mean kurtosis of the spectra of geostrophic norm (a) and geostrophic vorticity (b)

ysis for each area of study, at the monthly time scale over 2010.

5 Discussions

The results lead to the following discussions:

1. Differences in kurtosis (in particular, positive and negative) are significant and indicate different spectra. The norms of the velocity fields clearly show different turbulent properties between the norm of the oceanic velocity field with and without Ekman currents (i.e., considering wind stress forcing).

2. We note no significant difference in terms of vorticity spectra.

From these results we conclude that wind stress

does affect oceanic turbulence geographically, notably with respect to latitude. On vorticity, it is likely that other tools than the ones presented in this paper for the statistical study of turbulence have to be devised and tested.

6 Conclusions

In this paper, we have presented an experiment using daily, remotely sensed data acquired over one year to display different turbulence statistics of the oceanic system, with the goal of improving the description of the oceanic mesoscale (and sub-mesoscale) turbulence. Positive results put forward the differences in terms of wind stress according to

the area of study. The results confirm the usefulness of the multi-fractal formalism for the study of natural complex and turbulent acquired data. A turbulent regime classification for the world's oceans is very useful in adapting the turbulent cascade pathways toward a better inference of products for super-resolution currents (Yahia et al., 2010; Sudre et al., 2013). The methodology can also be adapted to high-resolution GHG fluxes (Garçon et al., 2013; Hernández-Carrasco et al., 2015, 2018). The study can be extended to build a monthly climatology with the 1993–2016 period of GEKCO products for each province, and globally.

References

- Arbic BK, Polzin KL, Scott JG, et al., 2013. On eddy viscosity, energy cascades, and the horizontal resolution of gridded satellite altimeter products. *J Phys Oceanogr*, 43(2):283-300. <https://doi.org/10.1175/jpo-d-11-0240.1>
- Arneodo A, Bacry E, Muzy JF, 1995. The thermodynamics of fractals revisited with wavelets. *Phys A*, 213(1-2):232-275. [https://doi.org/10.1016/0378-4371\(94\)00163-N](https://doi.org/10.1016/0378-4371(94)00163-N)
- Benzi R, Paladin G, Parisi G, et al., 1984. On the multi-fractal nature of fully developed turbulence and chaotic systems. *J Phys A*, 17:3521-3531. https://doi.org/10.1142/9789812799050_0017
- Boffetta G, Cencini M, Falconi M, et al., 2002. Predictability: a way to characterize complexity. *Phys Rep*, 356(6):367-474. [https://doi.org/10.1016/S0370-1573\(01\)00025-4](https://doi.org/10.1016/S0370-1573(01)00025-4)
- Chelton DB, Ries JC, Haines BJ, et al., 2001. Satellite altimetry. In: Fu LL, Cazenave A (Eds.), *Satellite Altimetry and Earth Sciences: a Handbook of Techniques and Applications*. Academic Press, London, UK, p.1-122.
- Frisch U, 1995. *Turbulence: the Legacy of A. N. Kolmogorov*. Cambridge University Press, Cambridge, UK.
- Garçon VC, Bell TG, Wallace D, et al., 2013. Perspectives and integration in SOLAS Science. In: Liss PS, Johnson MT (Eds.), *Ocean-Atmosphere Interactions of Gases and Particles*. Springer Berlin Heidelberg, p.247-306. https://doi.org/10.1007/978-3-642-25643-1_5
- Hernández-Carrasco I, Sudre J, Garçon V, et al., 2015. Reconstruction of super-resolution ocean pCO₂ and air-sea fluxes of CO₂ from satellite imagery in the southeastern Atlantic. *Biogeosciences*, 12(17):5229-5245. <https://doi.org/10.5194/bg-12-5229-2015>
- Hernández-Carrasco I, Garçon V, Sudre J, et al., 2018. Increasing the resolution of ocean pCO₂ maps in the South Eastern Atlantic Ocean merging multi-fractal satellite-derived ocean variables. *IEEE Trans Geosci Remote Sens*, in press. <https://doi.org/10.1109/TGRS.2018.2840526>
- Lee T, Stammer D, Awaji T, et al., 2010. Ocean state estimation for climate research. *Proc OceanObs'09: Sustained Ocean Observations and Information for Society*, p.1-9. <https://doi.org/10.5270/OceanObs09.cwp.55>
- Mashayek A, Ferrari R, Merrifield S, et al., 2017. Topographic enhancement of vertical turbulent mixing in the Southern Ocean. *Nat Commun*, 8:14197. <https://doi.org/10.1038/ncomms14197>
- Parisi G, Frisch U, 1985. On the singularity structure of fully developed turbulence. In: Ghil M, Benzi R, Parisi G (Eds.), *Turbulence and Predictability in Geophysical Fluid Dynamics*. North Holland, Amsterdam, p.84-87.
- She ZS, Leveque E, 1994. Universal scaling laws in fully developed turbulence. *Phys Rev Lett*, 72(3):336-339. <https://doi.org/10.1103/PhysRevLett.72.336>
- Sudre J, Maes C, Garçon V, 2013. On the global estimates of geostrophic and Ekman surface currents. *Limnol Oceanogr: Fluids Environ*, 3(1):1-20. <https://doi.org/10.1215/21573689-2071927>
- Turiel A, Pérez-Vicente CJ, Grazzini J, 2006. Numerical methods for the estimation of multi-fractal singularity spectra on sampled data: a comparative study. *J Comput Phys*, 216(1):362-390. <https://doi.org/10.1016/j.jcp.2005.12.004>
- Turiel A, Yahia H, Pérez-Vicente CJ, 2008. Microcanonical multi-fractal formalism—a geometrical approach to multi-fractal systems: Part I. Singularity analysis. *J Phys A*, 41(1):015501. <https://doi.org/10.1103/PhysRevE.74.061110>
- Turiel A, Isern-Fontanet J, Umbert M, 2014. Sensibility to noise of new multi-fractal fusion methods for ocean variables. *Nonl Processes Geophys*, 21(1):291-301. <https://doi.org/10.5194/npg-21-291-2014>
- Venugopal V, Roux SG, Foufoula-Georgiou E, et al., 2006. Revisiting multi-fractality of high-resolution temporal rainfall using a wavelet-based formalism. *Water Resour Res*, 42(6):W06D14. <https://doi.org/10.1029/2005WR004489>
- Yahia H, Sudre J, Pottier C, et al., 2010. Motion analysis in oceanographic satellite images using multiscale methods and the energy cascade. *Patt Recogn*, 43(10):3591-3604. <https://doi.org/10.1016/j.patcog.2010.04.011>